An Eulerian Vlasov code for plasma-wall interactions

2014 J. Phys.: Conf. Ser. 561 012005

(http://iopscience.iop.org/1742-6596/561/1/012005)

Journal of Physics: Conference Series **561** (2014) 012005 doi:10.1088/1742-6596/561/1/012005

An Eulerian Vlasov code for plasma-wall interactions

David Coulette and Giovanni Manfredi

Institut de Physique et Chimie des Matériaux de Strasbourg, CNRS and Université de Strasbourg, 23 rue du Loess, BP 43, F-67034 Strasbourg, France

E-mail: david.coulette@ipcms.unistra.fr, giovanni.manfredi@ipcms.unistra.fr

Abstract. In this work we present a new Eulerian kinetic 1D3V code devoted to the study of plasma-wall interactions and sheath structure. The code solves the Vlasov-Poisson system for two or more kinetic species on a one-dimensional spatial grid between two limiting plates, in the presence of a uniform magnetic field tilted with respect to the normal to the plates. A source-sink term in the Vlasov equation leads to a stationary solution comprising a magnetic and a collisional presheath, as well as the usual Debye sheath in front of the wall. Thanks to a nonuniform spatial grid the sheath structure can be resolved accurately. Several advection schemes are implemented and the code is parallelized. Here, the code is used to illustrate the problems of a stationary sheath-presheath structure in front of a negatively biased wall, with and without a tilted magnetic field.

1. Introduction

Despite the constant improvement of power and accessibility of computing resources, the accurate numerical simulation of plasma-wall interactions remains a challenging task. The intermixing of various time and space scales, dynamical regimes (from collisional to ballistic) and mutually-interacting multiple species, along with their nontrivial interactions with materials, lead to highly complex and costly modeling. As of today, the most comprehensive simulations are massively parallel PIC/Monte Carlo codes [1]. Such simulations have the advantage that atomic processes can be modeled in a straightforward way, but require heavy computational resources, since large numbers of macro-particles must be used to obtain reasonable accuracy. Accuracy is particularly hard to maintain in low-density regions such as the Debye sheaths. In contrast, Eulerian (Vlasov, Fokker-Planck) codes have the potential to fare better in those situations, as the distribution function is sampled with the same accuracy in all phase-space regions. However, they are computationally more demanding, and their treatment of collisions is more costly and less intuitive compared to PIC codes.

In this paper, we report on the latest advancements in the development of an Eulerian code for the study of the plasma-wall transition. We adopt a simplified geometry restricted to one dimension in space, with a uniform and constant magnetic field, while retaining full 3D velocity space description. The current implementation is a parallelized extension and generalization of the codes used in [2, 3, 4] to arbitrary number of species. As an illustration, we will show a few numerical results on the stationary sheath-presheath structure in front of a negatively biased wall, with and without a tilted magnetic field.

2. Model and code structure

2.1. Physical model

We consider a plasma bounded by two material plates (Fig. 1). The system is assumed to be invariant along the two coordinates parallel to the plates. The x direction, normal to the plates, may either represent the distance along the principal axis of a small linear machine, or the curvilinear coordinate along an open magnetic field line between divertor plates in a tokamak. The system is magnetized by a constant and uniform magnetic field $\mathbf{B}_0 = B_0(\sin\alpha\mathbf{e}_x + \cos\alpha\mathbf{e}_y)$. For each species, the dynamics is governed by the collisional Vlasov equation

$$\partial_t f_s + v_x \partial_x f_s + \frac{q_s}{m_s}(\mathbf{E} + \mathbf{v} \times \mathbf{B}_0) \cdot \boldsymbol{\nabla}_v f = \mathcal{C}_s + \mathcal{S}_s, \tag{1}$$

where $f_s(x, \mathbf{v})$ is the s^{th} species distribution function, $\mathcal{C}_s$ stands for the sum of all contributions from collisional processes, $\mathcal{S}_s$ is the sum of all independent sources, and $\mathbf{E} = -\partial_x \phi$ is the electrostatic field obtained self-consistently from the Poisson equation

$$-\partial_{xx}\phi = \sum_s \frac{q_s}{\epsilon_0} \int f_s d^3v. \tag{2}$$

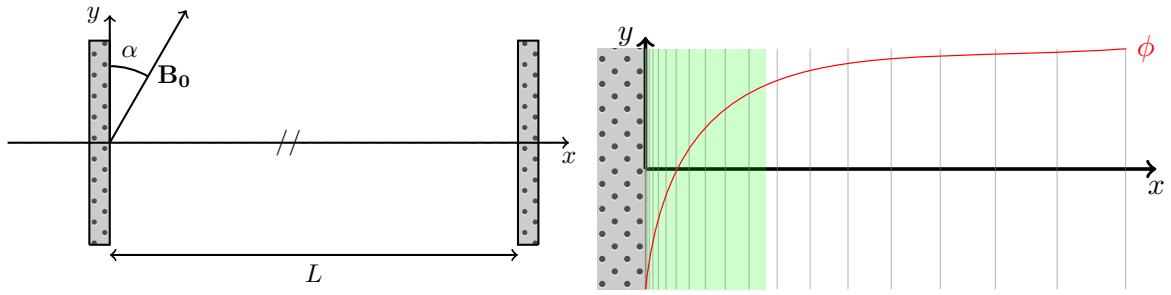

Figure 1. Model geometry (a) and non-uniform grid near the wall (b)

The distribution functions solution of Eq. (1) are assumed to be zero at all boundaries in velocity space ($\pm v_{\max}$). In the x direction, it is assumed that the incoming flux at the plates is zero (perfectly absorbing plate), but more complex boundary conditions can also be implemented to simulate particle-wall interactions such as physical sputtering or secondary electron emission. In some cases, only a half-infinite plasma will be considered, between one plate and a bulk position where the plasma is supposed to be at equilibrium.

Boundary conditions for the electrostatic potential at the plates may either be mixed Neumann/Dirichlet or Dirichlet/Dirichlet, which allows for the treatment of both floating and externally biased walls. When a full kinetic description is not necessary, the dynamics of some species (most often electrons) can follow a simplified model such as a Boltzmann law $n_s(x) = n_{s0} \exp\left[-(q_s(\phi - \phi_{ref})/k_B T_s\right]$, in which cases the Poisson equation becomes nonlinear and is solved iteratively.

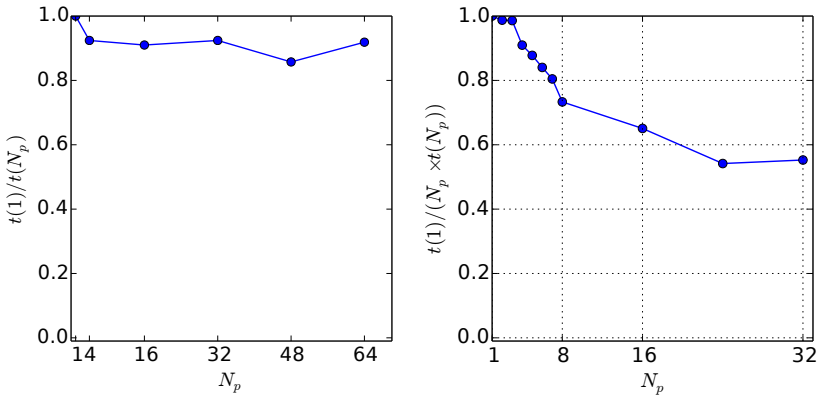

(a) (b)

Figure 2. Parallel efficiency of x domain decomposition (MPI): N_p is the number of MPI processes, $t(N_p)$ is the run duration. Efficiency $t(1)/t(N_p)$ scaling with growing global domain size $n_x = 64 \times N_p$ and $(n_{vx}, n_{vy}, n_{vz}) = (64, 64, 64)$ (a) and efficiency $t(1)/[N_p \times t(N_p)]$ scaling with a constant-size global domain $n_x = 1024$, $(n_{vx}, n_{vy}, n_{vz}) = (96, 96, 96)$ (b).

2.2. Numerical methods and implementation

Equation (1) is solved using a the following time-splitting scheme:

$$\begin{array}{rrl}
1: & \partial_t f_s + v_x \partial_x f_s = 0 & x \text{ advec. } (\Delta t) \\
2: & -\Delta\phi - \frac{1}{\epsilon_0}\rho = 0 & \text{Poisson solver} \\
3: & \partial_t f_s + \frac{q_s}{m_s}(E_x - B_y v_z)\partial_{v_x} f_s = 0 & v_x \text{ advec}(\Delta t) \\
4: & \partial_t f_s + \frac{q_s}{m_s}(B_x v_z)\partial_{v_y} f_s = 0 & v_y \text{ advec}(\Delta t) \\
5: & \partial_t f_s + \frac{q_s}{m_s}(B_x v_y - B_y v_x)\partial_{v_z} f_s = 0 & v_z \text{ advec.}(\Delta t) \\
6: & \partial_t f_s + \nu(f_s - F_0) = 0 & \text{BGK relaxation } (\Delta t)
\end{array} \tag{3}$$

where the advections in all four phase-space directions (steps 1, 3–5) and the source and collision terms (step 6) are treated sequentially.

Collisional processes are modeled using a single BGK relaxation operator acting as a restoring force that drives the distribution function towards a fixed Maxwellian $F_0 = n_{0s}\exp(-m_s v^2/2T_{0s})$. Thus $\mathcal{C}_s = -\nu(f_s - F_0)$, where ν is the relaxation rate.

All of the conservative advection equations take the simple linear form $\partial_t f + u_\xi \partial_\xi f = 0$, where $\xi \in \{x, v_x, v_y, v_z\}$ and u_ξ does not depend on ξ. They are integrated in time using a finite volume scheme [5] with reconstruction by primitive. Earlier versions of the code [2, 3, 4] used the flux-balanced scheme [6]. Several higher-order schemes have now been implemented and tested: (i) a fixed stencil polynomial interpolation with a choice of classical limiter functions, (ii) an ENO [7] scheme of arbitrary order, (iii) and a version of the PFC3 scheme [8] whose limiters have been modified to be used on a nonuniform grid. The latter is the default scheme in all results presented hereafter. It was selected as a good compromise between accuracy and computing effort.

The parallelization strategy relies on domain decomposition in the x dimension, implemented using MPI, and parallelization over species on each spatial sub-domain using OpenMP. This design does not fully exploit the parallelism that could be extracted by domain-decomposing the velocity dimensions. The rationale for this choice is to allow for the possibility of implementing more realistic collision operators. In that context, the full non-local coupling between velocity spaces of interacting species could lead to detrimental communication costs. Parallelization over

velocity dimensions, either by domain decomposition or fine-grained OpenMP parallelism, will thus be considered only once the collision operators framework is implemented.

Scalability tests were performed to evaluate the MPI parallel performance of the current design. The first (Fig. 2a) measures the so-called "weak" scaling: starting from a given spatial sub-domain size $n_x = 64$ with one MPI process $N_p = 1$, global domain size is constrained to grow linearly with the number of processes ($n_x = 64N_p$). The efficiency $e = t(1)/t(N_p)$ is measured against the ideal case, for which the runtime would be constant. The results show an acceptable scaling: the communication overhead is nearly constant in the tested N_p range. From a user point of view, it means that global domain size can be extended with no penalty.

The second test measures the "strong" scaling of efficiency. The global problem size is kept constant, while the number of sub-domains (and MPI processes) grows. The efficiency $e = t(1)/[N_p \times t(N_p)]$ is measured against the ideal case where runtime would scale as $1/N_p$. The results (Fig. 2b) show that the efficiency degrades and saturates with growing number of processes. The cost the Poisson solver [step 2 in Eq. (3)], which is parallelized using a block-decomposition scheme [9], stays negligible. Scalability is thus mostly limited by the x advection (step 1), for which the overhead brought forth by buffer exchange between sub-domains, redundant computation on overlapping regions, and all-to-all communications required by the PFC3 scheme become non-negligible with respect to the ideally parallel steps 3–6. From a user's perspective, and for "small" spatial domain sizes (typically a few hundred points), one can expect a maximal speed-up of about 10 to 20 without wasting computing resources.

3. Numerical results

We tested our code on two well-documented steady-state problems: the plasma-wall transition with and without a tilted magnetic field. In both cases, we considered a half-infinite plasma between an absorbing plate (located at $x = 0$) and a bulk plasma at equilibrium ($x = L$). The domain length is chosen to encompass several mean-free paths relatively to the BGK relaxation operator, so as to provide a smooth transition in the pre-sheath. At $t = 0$, the ion distribution is set to a spatially homogeneous Maxwellian with bulk parameters. During the evolution, governed by the Vlasov-Poisson equation, the ions are lost to the wall and the sheath forms rapidly. The system then evolves slowly until the balance between particle transport and the BGK relaxation is established in the presheath. The results shown in the forthcoming sections are all taken in this asymptotic steady-state regime.

3.1. Static sheath in a linear machine

First, we consider the steady state of a small linear machine filled with a non-magnetized argon plasma, leading to a simple 1D1V model. An analytical kinetic treatment of similar systems in a collisionless regime can be found in Refs. [11, 12]. The bulk plasma parameters ($n_e = n_i = 5.5 \times 10^{15}\mathrm{m}^{-3}$, $k_B T_i = 0.027\mathrm{eV}$, $k_B T_e = 2.5\mathrm{eV} \approx 100\mathrm{k_B T_i}$) were chosen to match those of Ref. [10]. In the actual machine, the wall potential is not driven by the bulk electrons, but by the highly energetic primary electrons emitted by the heated filament and then accelerated by a fixed discharge potential ($-50\mathrm{V}$ to $-100\mathrm{V}$). The wall bias then reaches values of the order of the discharge potential. As the density of primary electrons is three orders of magnitude lower than that of bulk electrons, their direct contribution to the space charge density is neglected. In order to mimic their impact on wall bias, we force the wall potential to values of the order of the discharge potential. This assumption makes it possible to reproduce the ion velocity profile observed in the experiment [10].

The bulk electrons are treated using a Boltzmann model. Additional simulations with kinetic electrons showed good agreement with the results obtained using the Boltzmann law. All collisional processes affecting the ions are modeled using a single BGK operator that forces

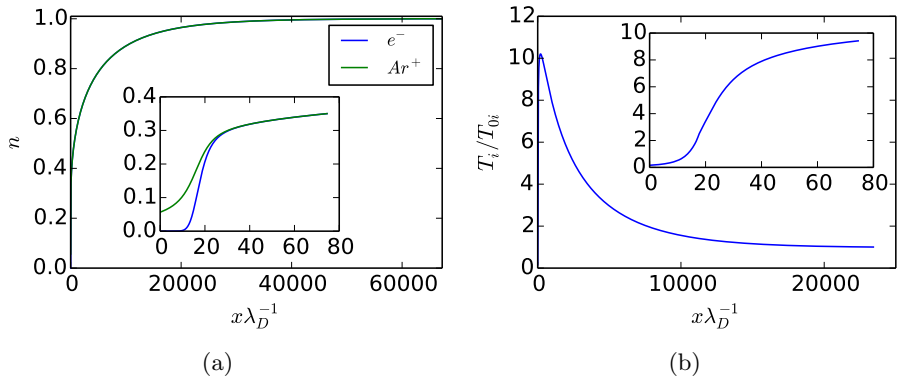

(a) (b)

Figure 3. Argon discharge steady-state with 50V wall bias and collision rate $\nu = 10^{-4}\omega_{pi}$: particles densities (a); ion temperature profile (b). The insets show zooms of the respective quantities.

the ion velocity distribution function (IVDF) to relax towards a Maxwellian with bulk plasma parameters, with a relaxation rate ν ranging from $\nu = 10^{-4}\omega_{pi}$ to $\nu = 10^{-2}\omega_{pi}$.

Although the model is simple, the actual parameters impose quite stringent requirements on the phase space resolution if one wants to describe accurately the evolution of the ion distribution function up to the wall. The required velocity range is governed by the wall potential, which is rather large compared to the ion bulk temperature. In the sheath, the ion distribution becomes very narrow, which requires even higher resolution, as both cell averaging and numerical diffusion tend to smear out the distribution profile. For this set of test cases, a $(n_x, n_{vx}) = (1024, 1024)$ grid has been used. The cell width in x ranges from $\Delta x = 0.01\lambda_D$ near the wall at $x = 0$ to $\Delta x = 100\lambda_D$ at the right boundary ($x \approx 2 \times 10^5\ \lambda_D$) where the plasma is at equilibrium

The density and temperature profiles are shown in Fig. 3. In the quasi-neutral pre-sheath, the ion behavior is dominated by the balance between plasma flow towards the wall and relaxation driven by the BGK term. The electric field tends to accelerate the ions towards the wall, whereas the BGK term tries to drag the ion distribution towards the equilibrium Maxwellian. The net result is that the ion velocity distribution widens in the presheath, leading to an increased kinetic temperature (Fig. 3b), defined as the velocity spread of the distribution function. The widening of the ion distribution in the presheath is clearly visible in Fig. 4a at position $x = 385\lambda_D$.

In the Debye sheath, characterized by strong charge separation (Fig. 3a) and strong electric fields (Fig. 4b), the effect of the BGK term is negligible, so that the ion trajectories are essentially ballistic. The ion distribution reduces to a cold beam that is strongly accelerated towards the wall, as can be seen in Fig 4a between $x = 18\lambda_D$ and $x = 0$. The thinning of the ion distribution is reflected in a drop of the ion kinetic temperature (Fig. 3b, inset).

In order to check that the chosen grid and interpolation scheme do not introduce any artificial widening of the distribution function, either by cell averaging or numerical diffusion, the simulation results are compared against an analytical ballistic model in the sheath (Fig. 5). Starting from a reference distribution function at the entrance of the sheath ($x = 34.3\lambda_D$), the ion distribution functions closer to the wall are obtained by conservation of the distribution along the characteristics. Although a slight erosion of the IVDF maximum can be seen (mostly due to the action of the limiters), the IVDF geometry, and most importantly its asymmetry, are well preserved by the PFC3 scheme, and spurious oscillations are controlled.

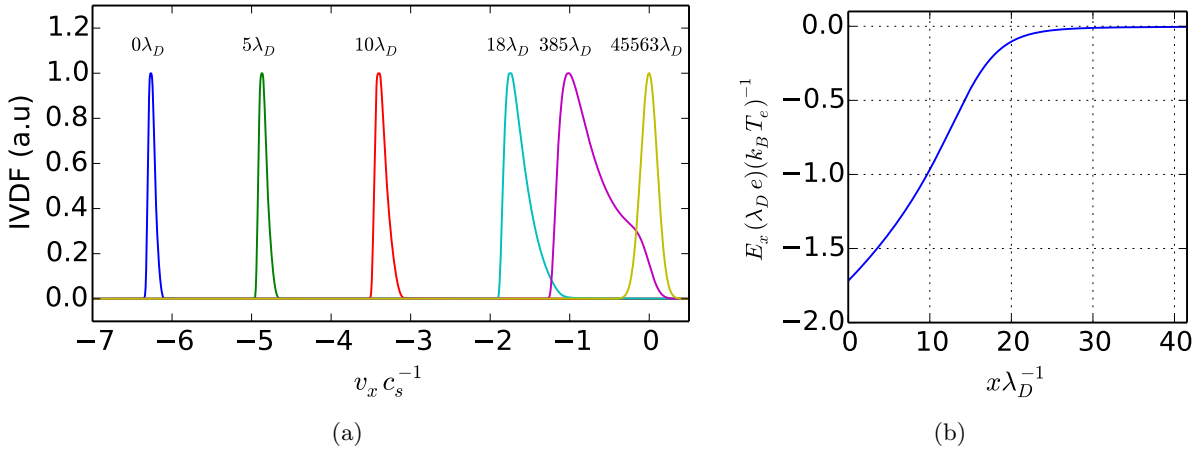

(a) (b)

Figure 4. Argon discharge with -50V wall bias and collision rate $\nu = 10^{-4}\omega_{pi}$. Evolution of the IVDF (normalized to its peak value) from the bulk plasma to the wall (a); distances from the wall are indicated above each peak. Electric field profile near the wall (b).

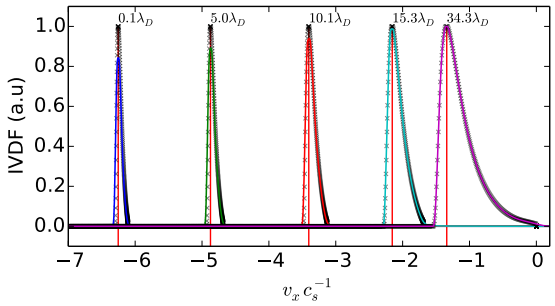

Figure 5. Argon discharge with a -50V wall bias and $\nu = 10^{-4}\omega_{pi}$. Evolution of the IVDF in the sheath: numerical results (continuous lines); IVDF computed from the reference profile at $x = 34.3\lambda_D$ using a ballistic model (crosses). The vertical lines mark the ballistic model peak velocity. All distributions are normalized to the peak value of the reference distribution at $x = 34.3\lambda_D$.

3.2. Magnetized deuterium plasma with tilted magnetic field

In order to test the operation of the code with a full 3D description in velocity space, we consider a deuterium plasma with kinetic ions and Boltzmann electrons. The setup is similar to the cases studied in Refs. [3, 4, 13, 14], with the geometry depicted in Figure 1. The discharge parameters are $T_e = T_i = 5$ eV, $\omega_{Ci} = 0.05\ \omega_{pi}$, $\alpha = 15°$, $\nu = 0.002\ \omega_{pi}$. The phase space is discretized on a $(256, 96, 96, 96)$ grid. The cell width ranges from $\Delta x = 0.5\lambda_D$ to $\Delta x = 500\lambda_D$, and the ion velocity range is $[-6v_{thi}; 6v_{thi}]$ in all directions. Albeit rather coarse, particularly in the sheath, this resolution is sufficient to obtain the main features of the collisional pre-sheath/magnetic pre-sheath/sheath transitions described in Ref. [13].

In a non-magnetized (or with normal incidence, $\alpha = 90°$) and weakly collisional plasma, the transition from the equilibrium bulk plasma to the quasi-ballistic regime in the sheath occurs in the collisional pre-sheath, where collisional/ionization processes compete with the ion flow towards the wall. In the magnetized plasma considered here, the magnetic field prevents the ions to flow directly towards the wall, particularly for grazing incidence.

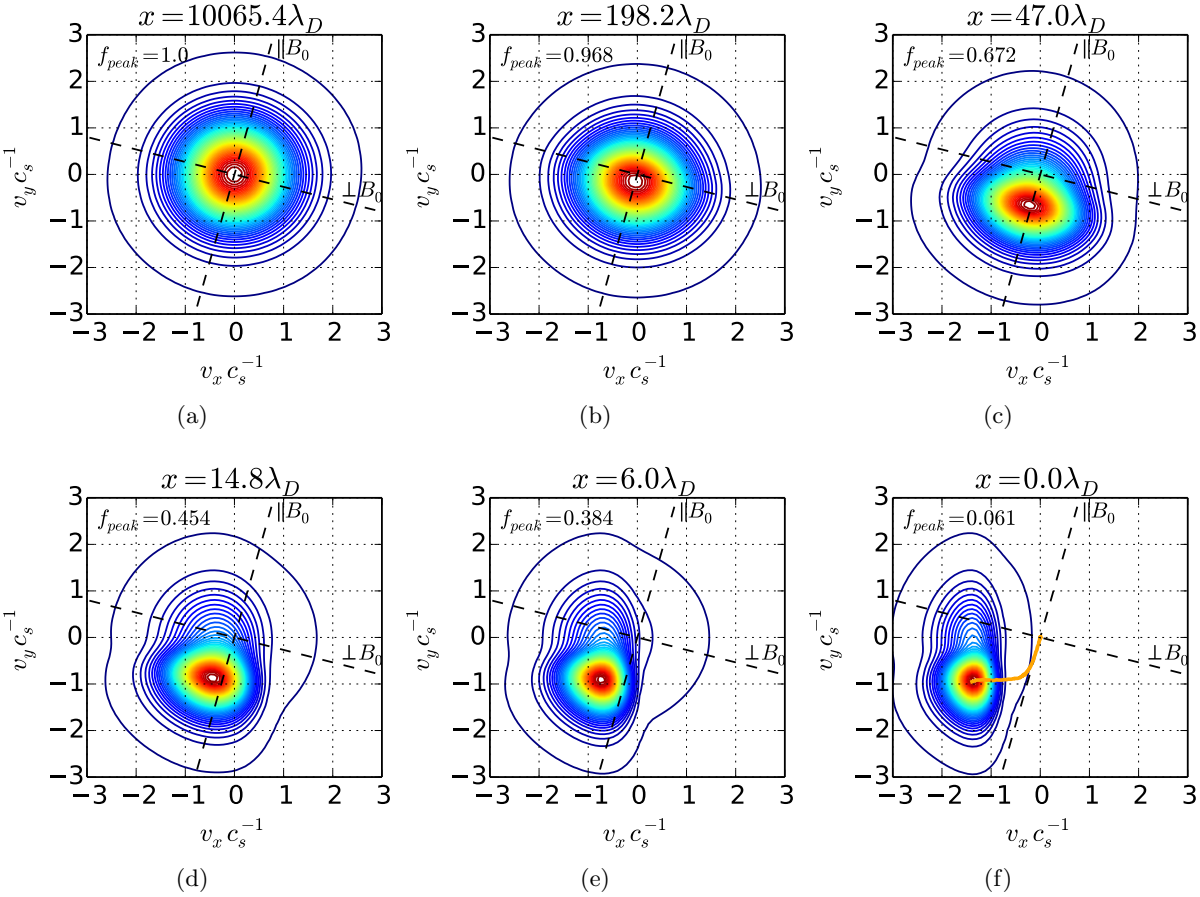

Figure 6. Contour plots of the v_z-averaged ion distributions normalized to their peak value (indicated in the upper left corner); dashed lines indicate the $\mathbf{B}_0$ and $\mathbf{e}_z \times \mathbf{B}_0$ directions. Bulk plasma (a); collisional pre-sheath (b-c); magnetic pre-sheath (d); Debye sheath (e); wall (f). The orange curve in (f) retraces the evolution of the peak of the distribution from the bulk plasma to the wall.

The overall transition from bulk to wall can be seen by looking at the evolution of the steady-state ion distribution function in the (v_x, v_y) plane (Fig. 6). In the collisional pre-sheath, as the ion mean velocity is slowly accelerated up to the sound speed, the magnetic field maintains the flow aligned with its own direction (Fig. 6a–c). In the magnetic pre-sheath, while the plasma is still quasi-neutral (Fig. 7b), the magnitude of the electric field is sufficient to break the alignment of the flow with the magnetic field (Fig. 6d). Eventually, the electric field dominates in the Debye sheath (Fig. 6e–f), where the ions are strongly accelerated in the direction normal to the wall.

The transition from the **B**-dominated pre-sheath to the **E**-dominated sheath is clearly visible in Fig. 7a, where we compare the magnitude of the various forces acting in the x direction. The Debye sheath entrance corresponds not only to the beginning of the nonneutral region (Fig. 7b), but also to the point where the electric force starts dominating over the Lorentz force $\mathbf{v} \times \mathbf{B}$.

4. Conclusion and perspectives

We presented the first developments of an Eulerian 1D3V code devoted to the study of plasma-wall interactions. Building up from earlier versions [3, 4], significant modifications were made

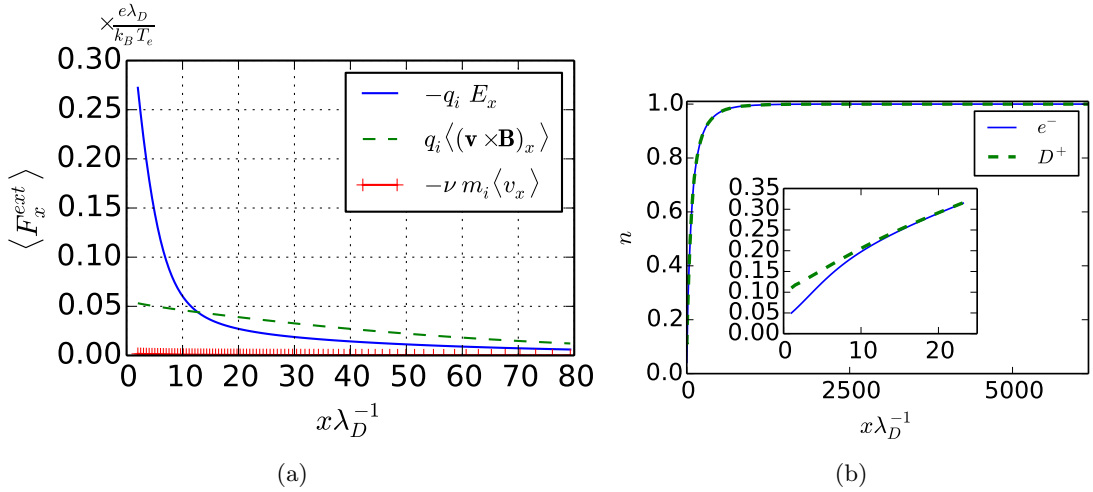

Figure 7. Deuterium plasma with tilted magnetic field, $\alpha = 15°$. Profiles of the various forces in the momentum balance equation (a). Note that the friction force $-\nu m_i \langle v_x \rangle$ caused by the BGK term is negligible over the whole domain. Density profiles for electrons and ions (b).

in order to adapt the code to its planned applications. Particle fluxes reaching the wall are the source of complex dynamics, including non-trivial feedback mechanisms, so that an accurate description of the distribution function must be preserved up to the wall. This necessity triggered the switch from the flux balance method to the PFC3 advection scheme. In addition, the present version can also address dynamical transient, and not only steady-state solutions, as was the case before [3, 4]. Finally, the parallelization over spatial sub-domains and different species opens the way to more demanding applications with acceptable run times.

Some standard cases, both in 1D1V and 1D3V, were used to check the validity and parallel performance of the code. The next steps will concentrate on the fully kinetic regime, in particular the comparison of Boltzmann and kinetic electron models for near-grazing incidence ($\alpha = 1-5°$) of the magnetic field. It is also planned to incorporate more accurate collision models than the simple BGK relaxation used so far. This is a major step, as it will introduce nontrivia integral terms in velocity space. Finally, more general plasma-wall effects should also be modeled, such as secondary-electron emission and sputtering from the wall [4].

Acknowledgements

The authors acknowledge the support of the French Agence Nationale de la Recherche (ANR) under reference ANR-12-BS09-028-01.

References

[1] Tskhakaya D and Kuhn S 2004 *Contrib. Plasma Phys.* **44** 564.
[2] Manfredi G and Valsaque F 2004 *Comp. Phys. Comm.* **164** 262.
[3] Devaux S and Manfredi G *Phys. Plasmas* **13** 083504.
[4] Devaux S and Manfredi G *Plasma Phys. Control. Fus.* **50** 025009.
[5] Leveque R.J 2004 *Finite Volume Methods for Hyperbolic Problems* ed. Cambridge University Press 387-95.
[6] Fijalkow E 1999 *Comp. Phys. Comm.* **116** 319.
[7] Abgrall R 1994 *J. Comp. Phys.* **114** 45.
[8] Filbet F, Sonnendrücker E and Bertrand P 2001 *J. Comp. Phys.* **172** 166.
[9] Polizzi E, Sameh A H 2006 *Parallel Computing* **32** 177.
[10] Claire N 2006 *Phys. Plasmas* **13** 062103.
[11] Emmert G A, Wieland R M Mense A T and Davidson J N 1980 *Phys. Fluids* **23** 803.

[12] Bissel R C, Johnson P C Stangeby PC 1989 *Phys. Fluids B* **1** 1133.
[13] Chodura R 1982 *Phys. Fluids* **25** 1628.
[14] Riemann K U 1994 *Phys. Plasmas* **1** 552.